



# Excellent thermal stability and low dielectric loss of $(\text{Ba}_{1-x}\text{Bi}_{0.5x}\text{Sr}_{0.5x})(\text{Ti}_{1-x}\text{Bi}_{0.5x}\text{Zr}_{0.5x})\text{O}_3$ solid solution ceramics in a broad temperature range applied in X8R

Xiaoxia Li<sup>1</sup> · Xiuli Chen<sup>1</sup> · Xiao Yan<sup>1</sup> · Huanfu Zhou<sup>1</sup> · Xiaobin Liu<sup>1</sup> · Xu Li<sup>1</sup> · Jie Sun<sup>1</sup>

Received: 13 August 2018 / Accepted: 16 October 2018 / Published online: 24 October 2018  
© Springer-Verlag GmbH Germany, part of Springer Nature 2018

## Abstract

$(\text{Ba}_{1-x}\text{Bi}_{0.5x}\text{Sr}_{0.5x})(\text{Ti}_{1-x}\text{Bi}_{0.5x}\text{Zr}_{0.5x})\text{O}_3$  [BBSTBZ,  $0.02 \leq x \leq 0.1$ ] ceramics were synthesized by a traditional solid-state reaction technique. The transition from tetragonal phase to pseudocubic phase at  $0.06 \leq x \leq 0.08$  was observed in Raman spectra and X-ray diffraction patterns. With adding ( $\text{Bi}^{3+}$ ,  $\text{Sr}^{2+}$ ,  $\text{Zr}^{4+}$ ), the thermal-stability of relative permittivity ( $\Delta\epsilon/\epsilon_{25^\circ\text{C}}$ ) and dielectric loss ( $\tan \delta$ ) of ceramics were optimized. Especially,  $(\text{Ba}_{0.9}\text{Bi}_{0.05}\text{Sr}_{0.05})(\text{Ti}_{0.9}\text{Bi}_{0.05}\text{Zr}_{0.05})\text{O}_3$  ceramics with small  $\Delta\epsilon/\epsilon_{25^\circ\text{C}}$  value ( $\leq \pm 15\%$ ) in a wide temperature range of  $-70^\circ\text{C}$  to  $155^\circ\text{C}$ , high  $\epsilon_r$  ( $\epsilon_r \sim 2088\text{--}2116$ ) and  $\tan \delta$  ( $\tan \delta \leq 0.02$ ) from  $-10^\circ\text{C}$  to  $200^\circ\text{C}$  were obtained, which indicates that BBSTBZ is suitable for X8R applications. Impedance spectroscopy was used to analyse the conduction and relaxation processes. The results showed that the relaxation and conduction process in the high-temperature region are thermally activated, and the oxygen vacancies are charge carriers.

## 1 Introduction

In recent years, the demand for multilayer ceramic capacitor (MLCC) has been increased rapidly. MLCC was used in modern electronic devices [1, 2]. For the application of the modern electronic devices, high working conditions demanded that the MLCCs have withstood higher operating temperature ( $\sim \geq 150^\circ\text{C}$ ). However, the ceiling temperature ( $\sim 125^\circ\text{C}$ ) of MLCCs for EIA (Electronic Industries Association) X7R (the change of the capacitance is less than 15% in the temperature range from  $-55$  to  $125^\circ\text{C}$ ) can not fulfill this requirement [3, 4]. Therefore, much attention has been paid to barium titanate to meet the needs of the X8R characteristics in which the change of the capacitance is less than 15% in the temperature range from  $-55$  to  $150^\circ\text{C}$  [5, 6].

However, pure barium titanate has the noticeable changes of permittivity near the Curie temperature ( $T_c \sim 130^\circ\text{C}$ ), which can not meet the temperature stability requirement in

the working temperature [7]. Generally, doping is an effective method to improve the performance of materials [8]. Many temperature-stable  $\text{BaTiO}_3$ -based dielectric materials have been developed, such as  $(1-x)\text{BaTiO}_3\text{-}x\text{Ba}(\text{Zn}_{0.5}\text{Ti}_{0.5})\text{O}_3$  [9–11];  $(1-x)\text{BaTiO}_3\text{-}x\text{Bi}(\text{Mg}_{0.5}\text{Zr}_{0.5})\text{O}_3$  [12];  $(1-x)\text{BaTiO}_3\text{-}x\text{LiTaO}_3$  [13]. These solid solution ceramics exhibit stable relative permittivity over a wide temperature range, which benefits to the high-temperature device applications.

Subsequently, the substitution of Zr for Ti was reported to improve the dielectric properties of BT ceramics [14]. In our previous work,  $\text{BaTiO}_3\text{-Bi}(\text{Mg}_{0.5}\text{Zr}_{0.5})\text{O}_3$  and  $\text{BaTiO}_3\text{-Bi}(\text{Li}_{0.33}\text{Zr}_{0.67})\text{O}_3$  showed good thermal stability of relative permittivity [15, 16]. Therefore, [ $\text{Bi}^{3+}$ ,  $\text{Sr}^{2+}$ ,  $\text{Zr}^{4+}$ ] (BSZ) were added to optimize the properties of  $\text{BaTiO}_3$  ceramic to satisfy the X8R characteristics in this work.  $(\text{Ba}_{1-x}\text{Bi}_{0.5x}\text{Sr}_{0.5x})(\text{Ti}_{1-x}\text{Bi}_{0.5x}\text{Zr}_{0.5x})\text{O}_3$  solid solution was designed and prepared by the solid-state reaction method. Moreover, the phase evolution, microstructure, impedance, and dielectric properties of ceramics were also studied.

✉ Xiuli Chen  
cxlnwpu@163.com

<sup>1</sup> Collaborative Innovation Center for Exploration of Hidden Nonferrous Metal Deposits and Development of New Materials in Guangxi, Key Laboratory of Nonferrous Materials and New Processing Technology, Ministry of Education, School of Materials Science and Engineering, Guilin University of Technology, Guilin 541004, China

## 2 Experimental

$(\text{Ba}_{1-x}\text{Bi}_{0.5x}\text{Sr}_{0.5x})(\text{Ti}_{1-x}\text{Bi}_{0.5x}\text{Zr}_{0.5x})\text{O}_3$  [BBSTBZ,  $0.02 \leq x \leq 0.1$ ] samples were synthesized by the traditional solid-state reaction technique as reported in our previous works [15, 16]. The samples were sintered at  $1280\text{--}1380^\circ\text{C}$

for 2 h in air. X-ray diffraction (XRD) patterns were studied at room temperature by an X-ray diffractometer (XRD, Model X'Pert PRO; PANalytical, Almelo, the Netherlands) with CuK $\alpha$  radiation ( $\lambda = 0.15406$  nm) operated at 40 kV and 40 mA with a step size of  $0.02^\circ$ . PanAnalytical software (X'PertHighscore Plus) was used to analyse the phase changes of XRD. Raman spectroscopy was carried out on a Thermo Fisher Scientific DXR using a 10 mW laser with a wave length of 532 nm. The microstructure of the samples sintered at their optimized temperatures was observed using a scanning electron microscope (Model JSM6380-LV SEM, JEOL, Tokyo, Japan). The silver paste is evenly applied to both sides of the sample plate, and heated up to  $700^\circ\text{C}$  for 30 min at a heating rate of  $3^\circ\text{C}/\text{min}$ . Dielectric properties were measured using a precision impedance analyzer (Model E4980AL, Hewlett–Packard Co, Palo Alto, CA) with an applied voltage of 500 mV over 100 Hz–1 MHz from  $-100$  to  $200^\circ\text{C}$  at a heating rate of  $2^\circ\text{C}/\text{min}$ .

### 3 Results and discussion

Figure 1 illustrates the XRD patterns of  $(\text{Ba}_{1-x}\text{Bi}_{0.5x}\text{Sr}_{0.5x})(\text{Ti}_{1-x}\text{Bi}_{0.5x}\text{Zr}_{0.5x})\text{O}_3$  [BBSTBZ,  $0.02 \leq x \leq 0.1$ ] ceramics sintered at their optimized temperatures. The main crystal phases of  $(\text{Ba}_{1-x}\text{Bi}_{0.5x}\text{Sr}_{0.5x})(\text{Ti}_{1-x}\text{Bi}_{0.5x}\text{Zr}_{0.5x})\text{O}_3$  ceramics ( $0.02 \leq x \leq 0.1$ ) were similar to the previous reports about the  $\text{BaTiO}_3$  [17, 18], suggesting that a homogenous solid solution was formed between the BSZ and BT. As  $0.02 \leq x \leq 0.06$ , the ceramics exhibited the tetragonal phase. With increasing the BSZ contents, the (002) and (200) peaks merged into a single (200) peak, indicating a transformation from tetragonal phase to pseudocubic phases [18]. As the

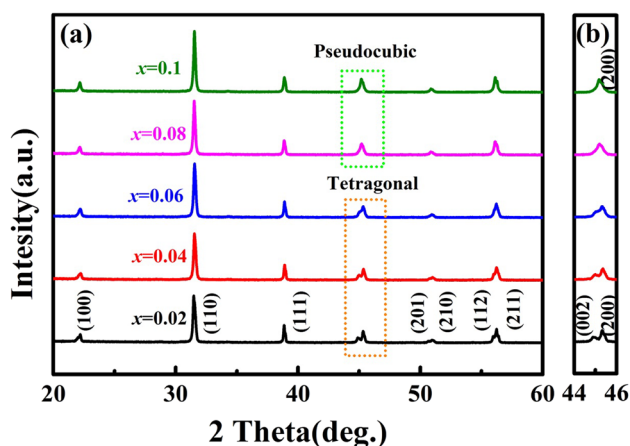


**Fig. 1** **a** X-ray diffraction patterns of  $(\text{Ba}_{1-x}\text{Bi}_{0.5x}\text{Sr}_{0.5x})(\text{Ti}_{1-x}\text{Bi}_{0.5x}\text{Zr}_{0.5x})\text{O}_3$  [BBSTBZ,  $0.02 \leq x \leq 0.1$ ] ceramics, **b** the enlarged XRD patterns of the samples in the range of  $2\theta$  from  $44^\circ$  to  $46^\circ$

$x$  values further increased, the (200) peak near  $45^\circ$  shifted significantly toward lower diffraction angles. This phenomenon demonstrated the expansion of lattices. The variation in lattice parameters as a function of  $(\text{Ba}_{1-x}\text{Bi}_{0.5x}\text{Sr}_{0.5x})(\text{Ti}_{1-x}\text{Bi}_{0.5x}\text{Zr}_{0.5x})\text{O}_3$  ceramics is demonstrated in Fig. 2. When  $x \leq 0.06$ , the parameter of  $a$  increased and  $c$  decreased with increasing  $x$ . As  $x = 0.08$ , the parameter of  $c$  became identical to  $a$ . As the  $x$  values further increased, the parameter of  $a$  and  $c$  increased. This variation is consistent with the shift of the (200) reflection toward lower diffraction angles, as illustrated in the enlarged XRD patterns of Fig. 1b.

This may be attributed to the fact that the ionic radii difference between  $(\text{Sr}^{2+} (1.44 \text{ \AA}, 12 \text{ coordinate}), \text{Bi}^{3+} (1.32 \text{ \AA}, 12 \text{ coordinate}))$  and  $\text{Ba}^{2+} (1.61 \text{ \AA}, 12 \text{ coordinate})$  are small in the A-site [19, 20]. But the B-site  $\text{Bi}^{3+} (1.03 \text{ \AA}, 6 \text{ coordinate})$  and  $\text{Zr}^{4+} (0.72 \text{ \AA}, 6 \text{ coordinate})$  are considerably larger than  $\text{Ti}^{4+} (0.605 \text{ \AA}, 6 \text{ coordinate})$  [21]. To further verify the occupation problem of Bi ions, the Rietveld refinement was carried out with the Pm-3m space group using GASA software, as shown in Fig. 3. For the refinements of BBSTBZ ( $x = 0.1$ ) ceramic phase structure, the coordinates of  $\text{BaTiO}_3$  were used as an initial model. The final refined data were listed in Table 1. The fitting parameters of  $P_{\text{wp}}$ ,  $R_p$ , and  $\chi^2$  values are 9.31%, 5.71%, and 9.4%, respectively, indicating that these values are reasonable. Based on the above fitting data, it can be also seen that one part of  $\text{Bi}^{3+}$  ions occupied A-site and the other part occupied B-site, which was consistent with the original stoichiometric design of the raw materials.

To clarify the phase evolution of  $(\text{Ba}_{1-x}\text{Bi}_{0.5x}\text{Sr}_{0.5x})(\text{Ti}_{1-x}\text{Bi}_{0.5x}\text{Zr}_{0.5x})\text{O}_3$  ( $0 \leq x \leq 0.1$ ) ceramics, Raman spectra in the frequency range of  $80\text{--}1000 \text{ cm}^{-1}$  at the room temperature are carried out, the results are listed in Fig. 4. The modes for  $x = 0$  were assigned as a single crystal

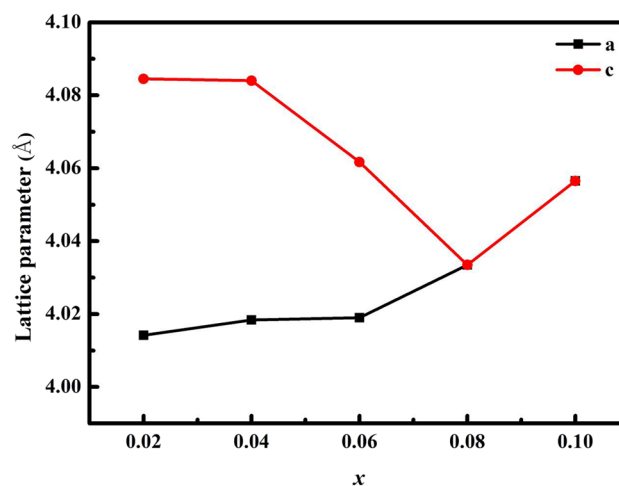


**Fig. 2** The variation in lattice parameters of  $(\text{Ba}_{1-x}\text{Bi}_{0.5x}\text{Sr}_{0.5x})(\text{Ti}_{1-x}\text{Bi}_{0.5x}\text{Zr}_{0.5x})\text{O}_3$  ceramics as a function of  $x$  values

**Table 1** Final refined structural parameters of  $(\text{Ba}_{0.9}\text{Bi}_{0.05}\text{Sr}_{0.05})(\text{Ti}_{0.9}\text{Bi}_{0.05}\text{Zr}_{0.05})\text{O}_3$

Atoms (Wyck.)	Occupancy	<i>x</i>	<i>y</i>	<i>z</i>	<i>B</i> <sub>iso</sub> (Å <sup>2</sup> )
Ba(1a)	0.9	0	0	0	0.013
Bi(1a)	0.05	0	0	0	0.025
Sr(1a)	0.05	0	0	0	0.001
Ti(1b)	0.9	0.5	0.5	0.5	0.015
Bi(1b)	0.05	0.5	0.5	0.5	0.02
Zr(1b)	0.05	0.5	0.5	0.5	0.8
O(3c)	1	0	0.5	0.5	0.014

Reliability factor: *R*<sub>wp</sub> = 8.31%, *R*<sub>p</sub> = 5.71%,  $\chi^2$  = 9.4%. Space group: Pm-3m

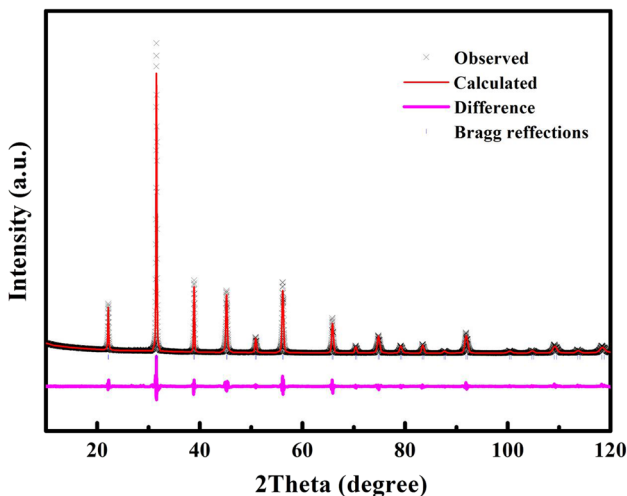


**Fig. 3** Rietveld refinement for  $(\text{Ba}_{0.9}\text{Bi}_{0.05}\text{Sr}_{0.05})(\text{Ti}_{0.9}\text{Bi}_{0.05}\text{Zr}_{0.05})\text{O}_3$  ceramic at room temperature

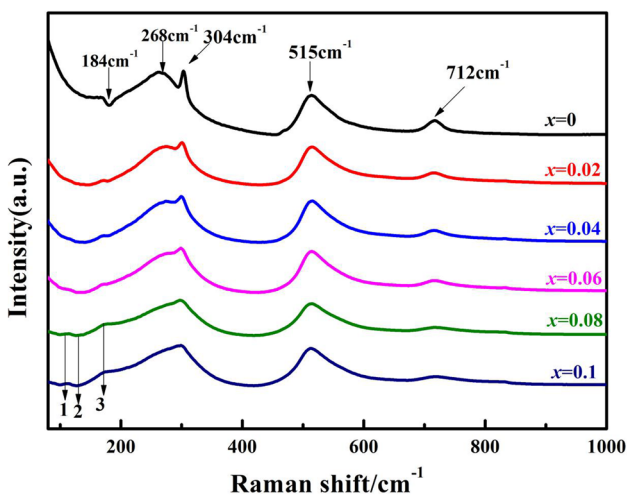


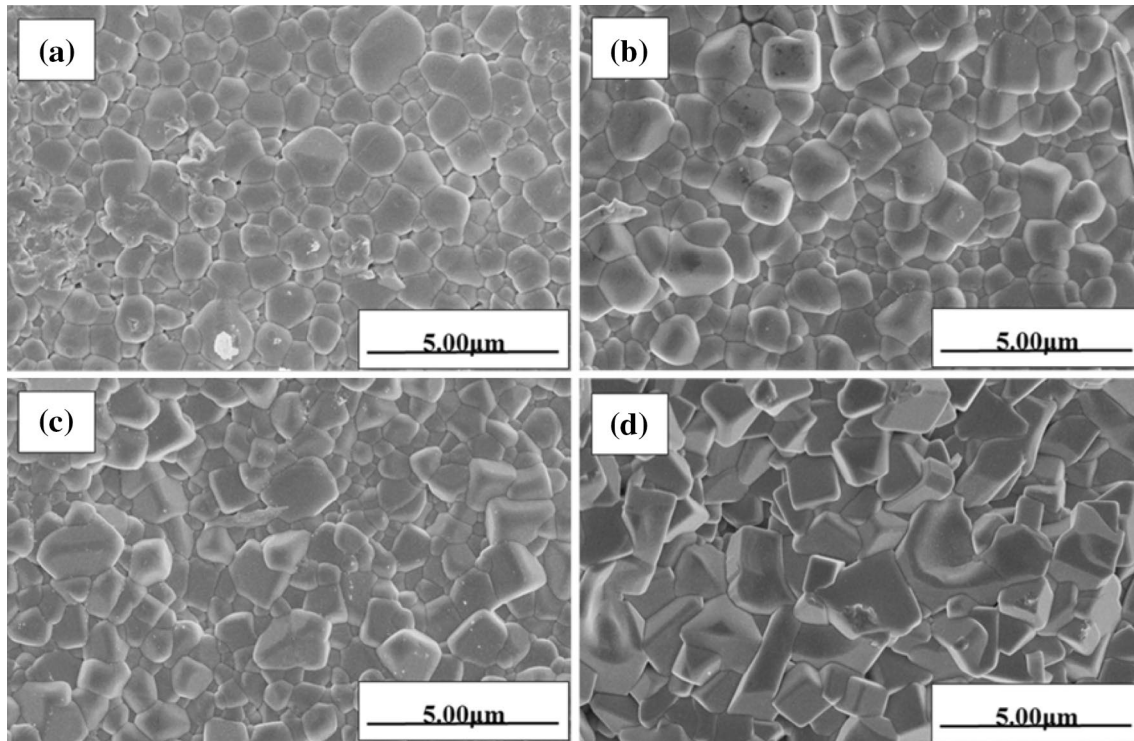
**Fig. 4** Room temperature Raman spectra of  $(\text{Ba}_{1-x}\text{Bi}_{0.5x}\text{Sr}_{0.5x})(\text{Ti}_{1-x}\text{Bi}_{0.5x}\text{Zr}_{0.5x})\text{O}_3$  [BBSTBZ,  $0 \leq x \leq 0.1$ ] ceramics

$\text{BaTiO}_3$ . When  $0 \leq x \leq 0.06$ , the main spectral features of  $(\text{Ba}_{1-x}\text{Bi}_{0.5x}\text{Sr}_{0.5x})(\text{Ti}_{1-x}\text{Bi}_{0.5x}\text{Zr}_{0.5x})\text{O}_3$  ceramics contained asymmetrically broad peaks at  $184 \text{ cm}^{-1}$ ,  $268 \text{ cm}^{-1}$ ,  $304 \text{ cm}^{-1}$ ,  $712 \text{ cm}^{-1}$  and symmetrically sharp peak at  $515 \text{ cm}^{-1}$ , which correspond to the  $\text{BaTiO}_3$  tetragonal phase [22, 23]. According to the previous reports [24, 25]. The Raman peak with positive intensity at  $180 \text{ cm}^{-1}$  is characteristic of the tetragonal phase. Besides, the other one around  $180 \text{ cm}^{-1}$  (appereived for  $x = 0.08, 0.1$ ) is indicative of the orthorhombic phase. These results are in good agreement with the XRD analysis. In addition, spectral characteristics have undergone tremendous changes in this range. The one at  $180 \text{ cm}^{-1}$  vanished and a new Model 3 appeared in its position. The vibrations of A-O could explain the Model 1 and Model 3, indicating the presence of  $\text{Ba}^{2+}$  or  $\text{Bi}^{3+}$  nano-sized regions [26]. The different sizes of octahedral interactions in the lattice would induce the appearance of Model 2 at low frequency.

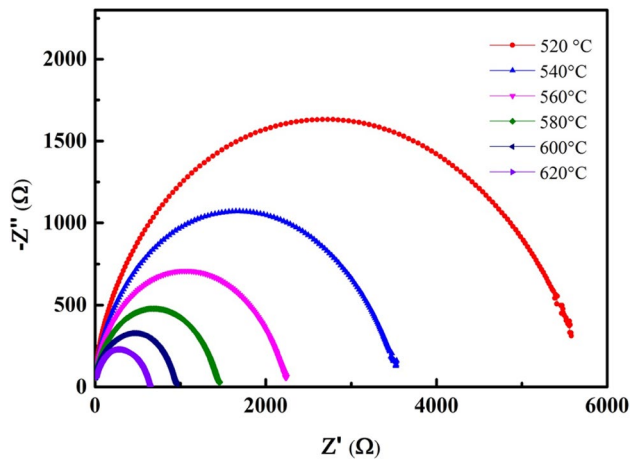
Figure 5 illustrates the SEM images of the natural surface for  $(\text{Ba}_{1-x}\text{Bi}_{0.5x}\text{Sr}_{0.5x})(\text{Ti}_{1-x}\text{Bi}_{0.5x}\text{Zr}_{0.5x})\text{O}_3$  ( $x = 0.02, 0.04, 0.08, 0.1$ ) ceramics sintered at their optimized temperatures. There were no significant differences for all compositions. As the BSZ contents increased, the grain size increased slightly, which indicates that BSZ could enhance the grain growth of the BBSTBZ ceramics. To elucidate the dielectric behavior of  $(\text{Ba}_{0.9}\text{Bi}_{0.05}\text{Sr}_{0.05})(\text{Ti}_{0.9}\text{Bi}_{0.05}\text{Zr}_{0.05})\text{O}_3$  ceramic, the high-temperature dielectric relaxation was studied by an impedance spectroscopy.

Figure 6 shows the Nyquist plots of the  $(\text{Ba}_{0.9}\text{Bi}_{0.05}\text{Sr}_{0.05})(\text{Ti}_{0.9}\text{Bi}_{0.05}\text{Zr}_{0.05})\text{O}_3$  ceramic at six temperatures. By increasing the measured temperature, the impedance decreases. Moreover, it is clearly observed that the center of the semi-circles is not located on the real axis, showing that the dielectric response of the  $(\text{Ba}_{0.9}\text{Bi}_{0.05}\text{Sr}_{0.05})(\text{Ti}_{0.9}\text{Bi}_{0.05}\text{Zr}_{0.05})\text{O}_3$  ceramic is slightly deviated from the pure Debye type relaxation. As the temperature increases, the resistance of the sample decreases, demonstrating that the conductivity increases.

Real (*Z'*) and imaginary (*Z''*) parts of the impedance as a function of the frequency and temperature for the  $(\text{Ba}_{0.9}\text{Bi}_{0.05}\text{Sr}_{0.05})(\text{Ti}_{0.9}\text{Bi}_{0.05}\text{Zr}_{0.05})\text{O}_3$  ceramic are illustrated in Fig. 7. The effects of the frequency and temperature on the *Z'* and *Z''* behaviors of the samples become clearly visible with increasing the frequency and temperature. With rising the frequency and temperature, the reduction of the *Z'* and *Z''* could be observed. And the values of these two parts at different temperatures are combined separately in high-frequency region, showing that the decrease in the barrier properties of the samples could lead to the release of the space charge with rising the measured temperature, which is the dominant factor in the increase of ac conductivity for samples at high temperatures [27]. At lower frequency, higher impedance value is a characteristic of the space



**Fig. 5** SEM micrographs of  $(\text{Ba}_{1-x}\text{Bi}_{0.5x}\text{Sr}_{0.5x})(\text{Ti}_{1-x}\text{Bi}_{0.5x}\text{Zr}_{0.5x})\text{O}_3$  ceramic sintered at their optimized temperatures: **a**  $x=0.02$ , 1360 °C, **b**  $x=0.04$ , 1340 °C, **c**  $x=0.08$ , 1300 °C, **d**  $x=0.1$ , 1280 °C



**Fig. 6** Nyquist plots of impedance of the  $(\text{Ba}_{0.9}\text{Bi}_{0.05}\text{Sr}_{0.05})(\text{Ti}_{0.9}\text{Bi}_{0.05}\text{Zr}_{0.05})\text{O}_3$  ceramics at selected temperatures

charge polarization for the materials, as shown in Fig. 7a. The low-frequency dispersion may be the thermally assisted electronic or ionic relaxation. By increasing the measured temperature, the value of  $Z''$  increases to a maximum, moves to a high frequency and becomes wide and generalized. The widened peak indicates the existence of temperature-dependent relaxation processes in the material, which may be due to the defects under high-temperature sintering [28].

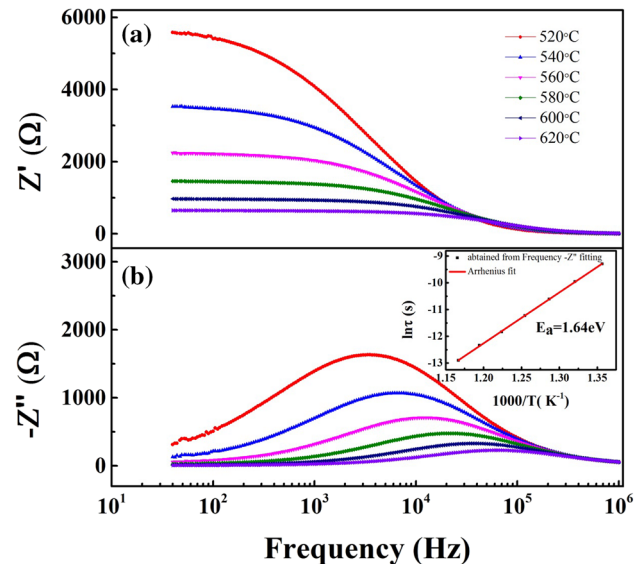


**Fig. 7** Frequency dependences of real part  $Z'$  (a) and imaginary part  $Z''$  (b) of impedance for  $(\text{Ba}_{0.9}\text{Bi}_{0.05}\text{Sr}_{0.05})(\text{Ti}_{0.9}\text{Bi}_{0.05}\text{Zr}_{0.05})\text{O}_3$  ceramics at selected temperatures [Insert shows the Arrhenius plot for relaxation time. The dotted line through the data is a linear fit to Eq. (2)]

Figure 7b shows the change in relaxation time as a function of the absolute temperature. In the relaxation system, the relaxation time ( $\tau$ ) can be calculated from the imaginary part ( $Z''$ ) and the frequency ( $f$ ) curve of the impedance (Fig. 7b). The following relationship was used:

$$\tau = \frac{1}{\omega} = \frac{1}{2\pi f_{\text{max}}} \tag{1}$$

where  $f_{\text{max}}$  is the relaxation frequency. According to Eq. (1), the value of  $\tau$  decreases with increasing temperature, which indicates a typical semiconductor behavior. The activation energy ( $E_a$ ) of this compound was calculated from the Arrhenius relation:

$$\tau = \tau_0 \exp(E_a/k_B T) \tag{2}$$

where  $\tau_0$  is the preexponential factor,  $k_B$  is the Boltzmann constant,  $E_a$  is the activation energy of relaxation, and  $T$  is the absolute temperature. From the slope of  $\log \tau$  vs  $10^3 T^{-1}$ , the activation energy of relaxation ( $E_a$ ) was 1.64 eV.

Figure 8 illustrates the normalized imaginary part of the impedance  $Z''/Z''_{\text{max}}$  as a function of the frequency and temperature. With the increase of temperature, the peaks of  $Z''/Z''_{\text{max}}$  move to high frequency. And the different positions of these peaks represent the significant charge polarization. The change in the apparent polarization is represented by the magnitude of mismatch between the peaks of the normalized parameters [29]. The localized conduction of multiple carriers would cause the polarization process, showing the presence of multiple relaxation process in materials. The different positions and the poor symmetry peaks of normalized parameters indicated the presence of short-range conductance [30]. As the temperature increases, the symmetry increases, indicating that the charge carriers migrate from short distance to long distance. As the temperature increases,

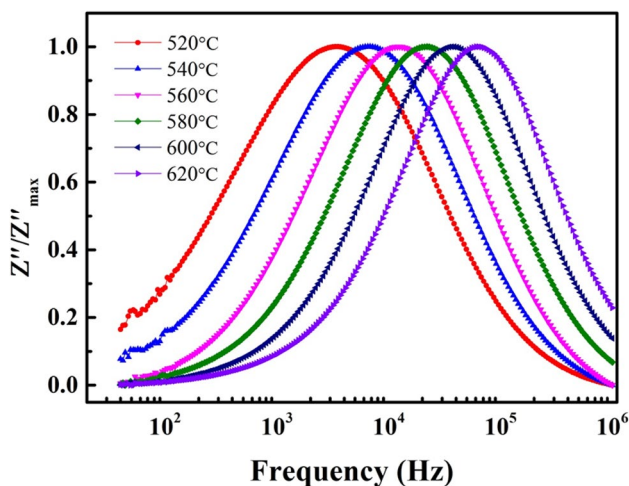


Fig. 8 Normalized imaginary parts,  $Z''/Z''_{\text{max}}$  of impedance as a function of frequency

the increase in long-distance conductivity is evidenced by the reduction of the volume resistance for materials, which is more clearly understood from the Nyquist curve.

The frequency dependence of the ac conductivity ( $\sigma_{\text{ac}}$ ) at six temperatures for  $(\text{Ba}_{0.9}\text{Bi}_{0.05}\text{Sr}_{0.05})(\text{Ti}_{0.9}\text{Bi}_{0.05}\text{Zr}_{0.05})\text{O}_3$  is shown in Fig. 9a. It can be seen that the  $\sigma_{\text{ac}}$  increases with increasing the frequency and temperature. With decreasing frequency, the  $\sigma_{\text{ac}}$  decreases and keeps a stable constant as the frequency increases to a certain value. Thence, the direct-current conductivity ( $\sigma_{\text{dc}}$ ) can be generated by extrapolating this part towards lower frequency. Moreover, it could be expressed through the universal dielectric response law [31]:

$$\sigma_{\text{ac}} = \sigma_{\text{dc}} + A\omega^n \tag{3}$$

where  $\sigma_{\text{dc}}$  is the dc conductivity,  $\omega$  is the angular frequency of ac field. The  $A$  and  $n$  ( $0 < n < 1$ ) are two temperature-dependent adjusting constants. The temperature dependence of the  $\sigma_{\text{dc}}$  was obtained by the Arrhenius law:

$$\sigma_{\text{dc}} = \sigma_0 \exp(-E_{\text{dc}}/k_B T) \tag{4}$$

where  $\sigma_0$  is the pre-exponential factor,  $E_{\text{dc}}$  is the activation energy of conduction and will be calculated from the slope of  $\log(\sigma)$  vs  $1000/T$ . The value is 1.26 eV. The dc conductivity increases with decreasing temperature. The activation energy of conduction is smaller than the activation energy of relaxation, which is consistent with previous reports [32].

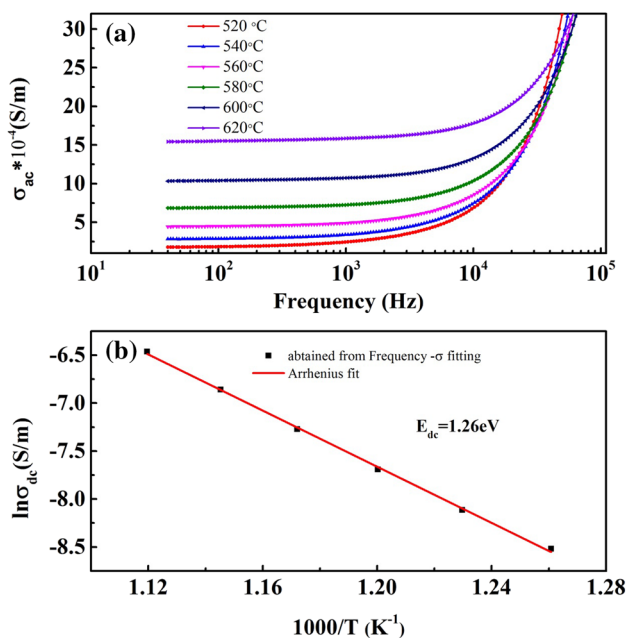
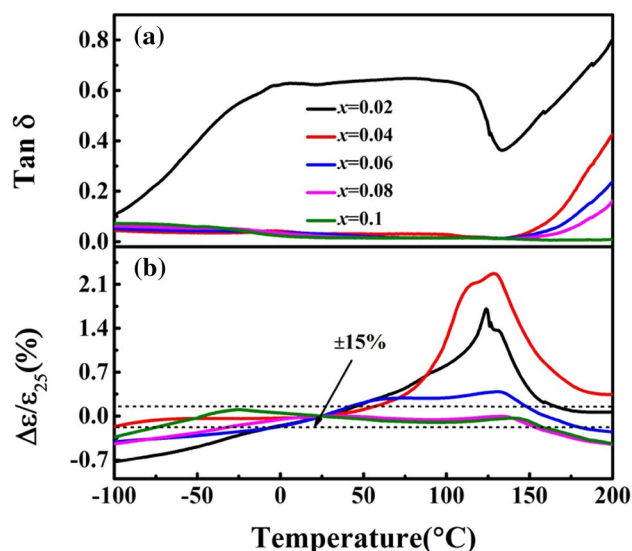
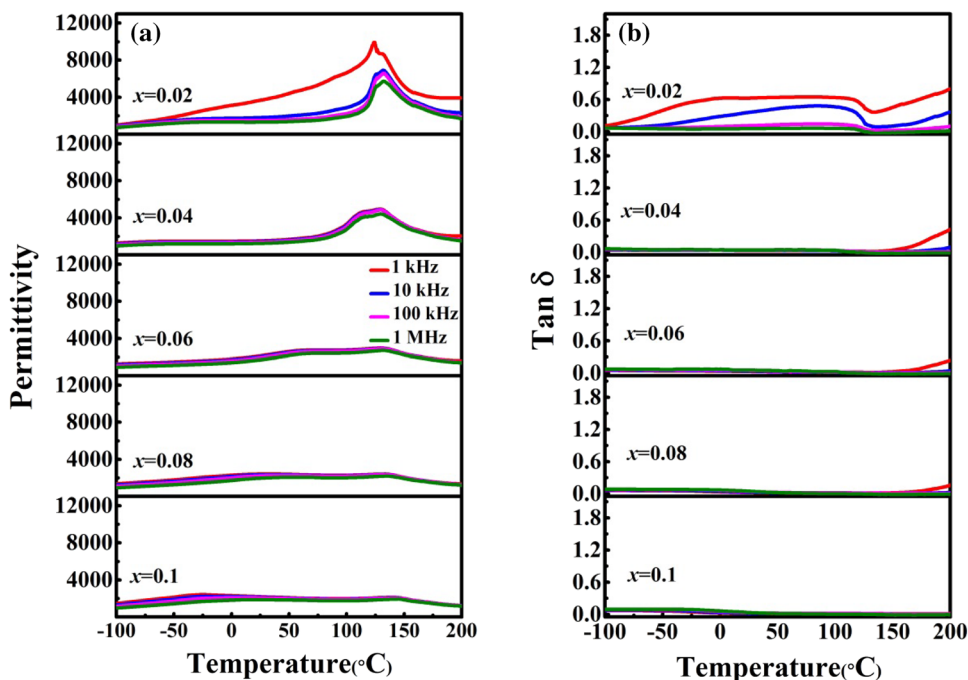


Fig. 9 a Frequency dependence of ac conductivity of the  $(\text{Ba}_{0.9}\text{Bi}_{0.05}\text{Sr}_{0.05})(\text{Ti}_{0.9}\text{Bi}_{0.05}\text{Zr}_{0.05})\text{O}_3$  ceramics at selected temperatures. b Arrhenius plot of dc conductivity for the  $(\text{Ba}_{0.9}\text{Bi}_{0.05}\text{Sr}_{0.05})(\text{Ti}_{0.9}\text{Bi}_{0.05}\text{Zr}_{0.05})\text{O}_3$ . Squares are experimental points and the dotted line is a linear fit to Eq. (4)

The activation energy of conduction includes the generation of carriers and the migration at a long distance, whereas the activation energy required for the relaxation of the carriers is due to the migration and jumping in adjacent lattice sites on the carriers. According to Steinsvik’s investigation [33], the changes of the activation energy for ABO<sub>3</sub> perovskite structure with the concentration of oxygen vacancies and the movement of the oxygen vacancies are considered to be a moving charge carrier in perovskite ferroelectrics [34]. And the charge compensation follows reaction [35]:  $V_O = V_{O''} + 2e'$  or  $V_{O'} = V_{O''} + e'$ . Double charge oxygen vacancies are considered most mobile charge and play an important role in conduction. And the direct-current conductivity is generated by the long-range movement of the double ionization oxygen vacancy [36].

Figure 10 demonstrates the temperature dependences of the relative permittivity ( $\epsilon_r$ ) and dielectric loss ( $\tan \delta$ ) for  $(Ba_{0.9}Bi_{0.05}Sr_{0.05})(Ti_{0.9}Bi_{0.05}Zr_{0.05})O_3$  ( $0.02 \leq x \leq 0.1$ ) ceramics in the measured temperature range from  $-100$  to  $200$  °C at 1 kHz, 10 kHz, 100 kHz and 1 MHz. With increasing the BSZ contents, the peak values of  $\epsilon_r$  reduced from  $\sim 9636$  ( $x=0.02$ , 10 kHz) to  $\sim 2116$  ( $x=0.1$ , 10 kHz). In addition, the  $\Delta\epsilon/\epsilon_{25\text{ }^\circ\text{C}}$  and the  $\tan \delta$  of  $(Ba_{1-x}Bi_{0.5x}Sr_{0.5x})(Ti_{1-x}Bi_{0.5x}Zr_{0.5x})O_3$  ( $0.02 \leq x \leq 0.1$ ) ceramics from  $-100$  to  $200$  °C at 10 kHz are illustrated in Fig. 11. As the BSZ contents increased, the  $\Delta\epsilon/\epsilon_{25\text{ }^\circ\text{C}}$  and  $\tan \delta$  got the ideal optimization. When  $x=0.1$ , the ceramics with the outstanding performances of small  $\Delta\epsilon/\epsilon_{25\text{ }^\circ\text{C}}$  values ( $\pm 15\%$ ) in the temperature range from  $-70$  to  $155$  °C and  $\tan \delta \leq 0.02$  in the temperature range from  $-10$  to  $200$  °C were obtained. Therefore, the  $\Delta\epsilon/\epsilon_{25\text{ }^\circ\text{C}}$ , temperature dependence

**Fig. 10** Temperature dependence of relative permittivity and dielectric loss for  $(Ba_{1-x}Bi_{0.5x}Sr_{0.5x})(Ti_{1-x}Bi_{0.5x}Zr_{0.5x})O_3$  [BBSTBZ,  $0.02 \leq x \leq 0.1$ ] ceramics measured at 1 kHz, 10 kHz, 100 kHz and 1 MHz



**Fig. 11** a  $\Delta\epsilon/\epsilon_{25\text{ }^\circ\text{C}}$  of  $(Ba_{1-x}Bi_{0.5x}Sr_{0.5x})(Ti_{1-x}Bi_{0.5x}Zr_{0.5x})O_3$  [BBSTBZ,  $0.02 \leq x \leq 0.1$ ] ceramics at 10 kHz, b dielectric loss of  $(Ba_{1-x}Bi_{0.5x}Sr_{0.5x})(Ti_{1-x}Bi_{0.5x}Zr_{0.5x})O_3$  [BBSTBZ,  $0.02 \leq x \leq 0.1$ ] ceramics at 10 kHz

of  $\epsilon_r$  and  $\tan \delta$  for  $(Ba_{0.9}Bi_{0.05}Sr_{0.05})(Ti_{0.9}Bi_{0.05}Zr_{0.05})O_3$  ceramics at 1, 10, and 100 kHz from  $-100$  to  $200$  °C are shown in Fig. 12. The  $(Ba_{0.9}Bi_{0.05}Sr_{0.05})(Ti_{0.9}Bi_{0.05}Zr_{0.05})O_3$  ceramics with small  $\Delta\epsilon/\epsilon_{25\text{ }^\circ\text{C}}$  values ( $\pm 15\%$ ) in the wide temperature range of  $-70$  to  $155$  °C at the frequency range from 1 kHz to 10 kHz,  $\tan \delta \leq 0.02$  from  $-10$  to  $200$  °C, and high  $\epsilon_r$  ( $\sim 2088$ – $2116$ ) were obtained, showing

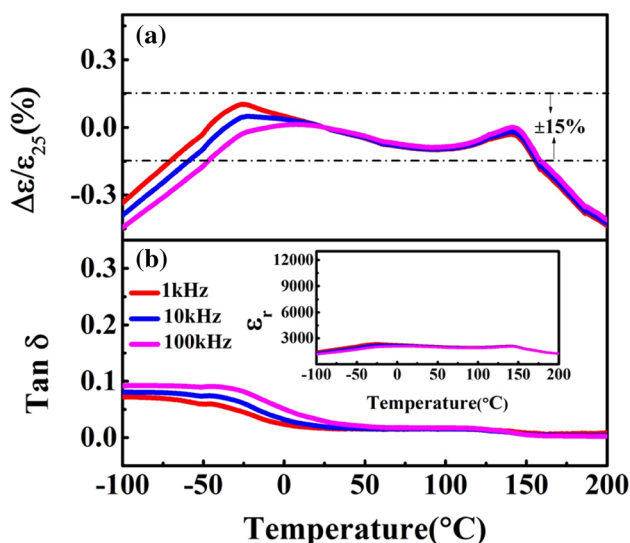


**Fig. 12** **a**  $\Delta\epsilon/\epsilon_{25}$  of  $(\text{Ba}_{1-x}\text{Bi}_{0.5x}\text{Sr}_{0.5x})(\text{Ti}_{1-x}\text{Bi}_{0.5x}\text{Zr}_{0.5x})\text{O}_3$  ( $x=0.1$ ) ceramics at 1, 10, 100 kHz from  $-100$  to  $200$  °C, **b** temperature dependence of relative permittivity, and dielectric loss of  $(\text{Ba}_{1-x}\text{Bi}_{0.5x}\text{Sr}_{0.5x})(\text{Ti}_{1-x}\text{Bi}_{0.5x}\text{Zr}_{0.5x})\text{O}_3$  ( $x=0.1$ ) ceramics at 1, 10, 100 kHz from  $-100$  to  $200$  °C

that  $(\text{Ba}_{1-x}\text{Bi}_{0.5x}\text{Sr}_{0.5x})(\text{Ti}_{1-x}\text{Bi}_{0.5x}\text{Zr}_{0.5x})\text{O}_3$  ceramics can be used in X8R MLCCs.

## 4 Conclusions

$(\text{Ba}_{1-x}\text{Bi}_{0.5x}\text{Sr}_{0.5x})(\text{Ti}_{1-x}\text{Bi}_{0.5x}\text{Zr}_{0.5x})\text{O}_3$  ( $0.02 \leq x \leq 0.1$ ) lead-free ceramics have been investigated using the conventional solid-state processing techniques. The systematically structural transformation from tetragonal to pseudo cubic phase occurred at  $0.06 \leq x \leq 0.08$ . As the BSZ contents increased, the peak  $\epsilon_m$  values with the broadening of tetragonal-cubic transition peaks were significantly reduced. The  $(\text{Ba}_{0.9}\text{Bi}_{0.05}\text{Sr}_{0.05})(\text{Ti}_{0.9}\text{Bi}_{0.05}\text{Zr}_{0.05})\text{O}_3$  ceramics showed the outstanding dielectric performances with small  $\Delta\epsilon/\epsilon_{25}$  values ( $\pm 15\%$ ) in the temperature range of  $-70$  to  $155$  °C, high  $\epsilon_r$  ( $\sim 2088$ – $2116$ ) and  $\tan \delta \leq 0.02$  from  $-10$  to  $200$  °C. The impedance spectroscopy showed that the relaxation and the conduction process in the high-temperature region are thermally activated, and the oxygen vacancies are charge carriers.

**Acknowledgements** This study was supported by Natural Science Foundation of China (Nos. 11464009 and 11664008), Natural Science Foundation of Guangxi (Nos. 2015GXNSFDA139033, 2017GXNS-FFA198011 and 2017GXNSFDA198027) and Research Start-up Funds Doctor of Guilin University of Technology (No. GUTQDJJ2017133).

## References

1. Y.M. Zhang, M.H. Cao, Z.H. Yao, Z.J. Wang, Z. Song, A. Ullah, H. Hao, H.X. Liu, Mater. Res. Bull. **67**, 70–76 (2015)
2. J. Wang, S.L. Jiang, D. Jiang, J.J. Tian, Y.L. Li, Y. Wang, Mater. Res. Bull. **38**, 5853–5857 (2012)
3. S.F. Wang, G.O. Dayton, J. Am. Ceram. Soc. **82**, 2677–2682 (2010)
4. W.H. Lee, C.Y. Su, J. Am. Ceram. Soc. **90**, 3345–3348 (2010)
5. V. Gartnerova, O. Pacherova, M. Klinger, M. Jelinek, A. Jager, M. Tyunina, Mater. Res. Bull. **89**, 180–184 (2017)
6. Y.H. Hoon, Y.H. Han, Jpn. J. Appl. Phys. **44**, 6143 (2014)
7. T. Ishidate, S. Abe, H. Takahashi, N. Mori, Phys. Rev. Lett. **78**, 2397–2400 (1997)
8. Y.J. Wu, Y.Q. Lin, S.P. Gu, X.M. Chen, Appl. Phys. A Mater. Sci. Process. **97**, 191–194 (2009)
9. J.B. Lim, S. Zhang, T.R. Shrout, Electron. Mater. Lett. **7**, 71–75 (2011)
10. T. Wang, H. Hao, M. Liu, D. Zhou, Z. Yao, M. Cao et al., J. Am. Ceram. Soc. **98**, 690–693 (2015)
11. N. Raengthon, H.J. Brown-Shaklee, G.L. Brennecka, D.P. Cann, J. Mater. Sci. **48**, 2245–2250 (2013)
12. A. Zeb, S.J. Milne, J. Eur. Ceram. Soc. **34**, 3159–3166 (2014)
13. S.F. Wang, J.H. Li, Y.F. Hsu, Y.C. Wu, Y.C. Lai, M.H. Chen, J. Eur. Ceram. Soc. **33**, 1793–1799 (2013)
14. S. Mahajan, D. Haridas, K. Sreenivas, O.P. Thakur, C. Prakash, Mater. Lett. **97**, 40–43 (2013)
15. X.L. Chen, J. Chen, D.D. Ma, L. Fang, H.F. Zhou, Ceram. Int. **41**, 2081–2088 (2015)
16. X.L. Chen, G.S. Huang, D.D. Ma, G.F. Liu, H.F. Zhou, Ceram. Int. **43**, 926–929 (2017)
17. D.D. Ma, X.L. Chen, G.S. Huang, J. Chen, H.F. Zhou, F. Fang, Ceram. Int. **41**, 7157–7161 (2015)
18. K. Suzuki, K. Kijima, J. Mater. Sci. **40**, 1289–1892 (2005)
19. C.C. Huang, D.P. Cann, X. Tan, N. Vittayakorn, J. Appl. Phys. **102**, 136 (2007)
20. R.D. Shannon, Acta Crystallogr. A **32**, 751–767 (1976)
21. C.B. Long, H.Q. Fan, M.M. Li, G.Z. Dong, Q. Li, Scr. Mater. **75**, 70–73 (2014)
22. M. Deluca, Z.G. Al-Jlaihawi, K. Reichmann, A.M.T. Bell, A. Feteira, J. Mater. Chem. A **6**, 5443–5451 (2018)
23. U.D. Venkateswaran, V.M. Naik, R. Naik, Phys. Rev. B **58**, 14256–14260 (1998)
24. C.H. Perry, D.B. Hall, Phys. Rev. Lett. **15**, 700–702 (1965)
25. M.H. Frey, and D.A. Phys. Rev. B **54**, 3158 (1996)
26. J. Kreisel, P. Bouvier, M. Maglione, B. Dkhil, A. Simon, Phys. Rev. B **69**, 092104 (2004)
27. J. Plocharski, W. Wiczorek, Solid. State. Ionics. **28**, 979–982 (1988)
28. A.K. Jonscher, The universal dielectric response. Nature. **6**, 19–24 (1977)
29. R. Gerhardt, J. Phys. Chem. Solids **55**, 1491–1506 (1994)
30. X. Yao, Z.L. Chen, L.E. Cross, J. Appl. Phys. **54**, 3399–3403 (1984)
31. A.K. Jonscher, J. Phys. D Appl. Phys. **32**, R57–R70 (1999)
32. L. Liu, Y. Huang, Y. Li, M. Wu, L. Fang, C. Hu, Y. Wang, Phys. B **407**, 136–139 (2012)
33. S. Steinsvik, R. Bugge, J. Gjønnes, J. Taftø, T. Norby, J. Phys. Chem. Solids **58**, 969–976 (1997)
34. S. Sen, R. Choudhary, P. Pramanik, Phys. B **387**, 56–62 (2007)
35. F.A. Kröger, H.J. Vink, J. Phys. Chem. Solids **5**, 208–223 (1958)
36. C. Ang, Z. Yu, L.E. Cross, Phys. Rev. B. **62**, 228–236 (2000)